Automation in Construction 71 (2016) 13–20

Contents lists available at ScienceDirect

Automation in Construction

journal homepage: www.elsevier.com/locate/autcon

Inertial measurement unit based indoor localization for construction applications

Magdy Ibrahim [a,*], Osama Moselhi [b]

[a] Department of Civil & Environmental Engineering, University of Waterloo, Ontario, Canada
[b] Department of Building, Civil & Environmental Engineering, Concordia University, Montréal, Québec, Canada

ARTICLE INFO

Article history:
Received 1 October 2015
Received in revised form 1 April 2016
Accepted 4 May 2016
Available online 25 May 2016

Keywords:
Indoor localization
IMU
Automated progress reporting
Inertial navigation
Kalman filter
DCM

ABSTRACT

Localization and tracking of resources on construction jobsites are an emerging area where the location of materials, labor, and equipment is used to estimate productivity, measure project's progress and/or enhance jobsite safety. GPS has been widely used for outdoor tracking of construction operations. However, GPS is not suitable for indoor applications due to the lack of signal coverage; particularly inside tunnels or buildings. Several indoor localization research studies had been attempted, however such developments rely heavily on extensive external communication network infrastructures. These developments also are susceptible to electromagnetic interference in noisy construction jobsites. This paper presents indoor localization system using a microcontroller equipped with an inertial measurement unit (IMU). The IMU contains a cluster of sensors: accelerometer, gyroscope and magnetometer. The microcontroller uses a direct cosine matrix algorithm to fuse sensors data and calculate non-gravitational acceleration using nine-degrees-of-freedom motion equations. Current position is calculated based on measured acceleration and heading, while accounting for growing error in speed estimation utilizing jerk integration algorithm. Experimental results are presented to illustrate the relative effectiveness of the developed system, which is able to operate independently of any external aids and visibility conditions.

1. Introduction

The fact that indoor localization research is to date a very active research area indicates that there are still many challenges left to resolve. The challenges depend on the required accuracy and reliability dictated by the application. Recent advances in sensing technologies have enabled the deployment of a wide range of technologies for identification, location sensing, and tracking of resources. Consequently many research works had been developed for asset tracking, earthmoving operations, surveying, safety hazards predicting, and context aware construction [1–10].

Over the past few years, several researchers have experimented with indoor positioning technologies, which can be grouped in three major categories: (1) wave propagation; (2) image based; and (3) inertial navigation. Wave propagation technologies are based on the physical propagation properties of radio, ultrasonic or sound waves over distances [11–16]. Ultra wideband, infrared, WLAN and RFID are examples for radio frequency (RF) localization technology. However, even if they suffer from several limitations, infrared technology provides room-level accuracy and performs poorly in the presence of sunlight [16]. WLAN technology localization accuracy had been investigated by different researchers, and found to be varying from 4 to 9 m depending on localization algorithm utilized and number of WLAN access points [17–19]. Varying accuracies of RFID localization systems had been reported by researchers, from 5 to 9 m depending on the tags' configuration and the density of tag deployment [20–22]. Ultra wideband-based systems have a very high accuracy of approximately 20 cm [23], however the cost of commercially available ultra wideband localization systems is very high. Ultrasound technology is based on sound wave propagation. The reported accuracy of an ultrasound system is 9 cm [23], however, it requires line of sight for deployment of transmitters, and the cost is comparable to ultra wideband transmitters [16]. Narrow Bandwidth Phase Analysis is an emerging radio frequency based technology for indoor localization, which is based on a high-resolution spectral analyzing method to measure the phase differences of a set of 2.4 GHz frequencies, with an average localization accuracy of 1.26 m [24].

Image-based localization technology involves image matching and computer vision techniques. Computer vision techniques have been categorized as (1) global methods such as edge detection and feature recognition, and (2) local methods based on landmark detection using visual tags or image matching [25]. However, these methods yield coarse accuracy (room-level) and are susceptible to occlusions and changes in the environment.

Inertial navigation localization technology utilizes an accelerometer and a gyroscope for sensing and detecting motion. The accelerometer measures acceleration in three dimensional spaces. The displacement

* Corresponding author. Tel.: +1 514 632 5080.
E-mail addresses: magdy.omar@yahoo.com (M. Ibrahim), moselhi@encs.concordia.ca (O. Moselhi).

http://dx.doi.org/10.1016/j.autcon.2016.05.006
0926-5805/

is calculated by double integration of the acceleration. The gyroscope combined with the accelerometer is used to calculate the heading. This principle is called dead reckoning technique [26]. The dead reckoning is based on fusing the acceleration, and heading direction during a time step to determine how far and in what direction the user has moved from last known position. Unlike WLAN and RFID, motion sensing technology is independent from any infrastructure [27]. However, accelerometers are susceptible to acceleration caused by random movements, which might not necessarily be human motion, and magnetometers are susceptible to magnetic fields generated by electrical equipment and electronics [27]. Overall, motion sensing does not provide high location accuracies, but the accuracy can be improved by smart algorithms, which are able to correct drift errors [28].

Several methods recently developed to compensate the inherited errors in inertial navigation system by integrating different technologies and algorithms. A fusion of IMU and RGB-D camera based visual gyroscope is utilized to avoid the drift errors in common gyroscope sensors [29]. Twice position-fix reset (TPR) method is introduced recently to improve the accuracy of a dual-axis rotational INS for long term navigation applications [30]. The TPR method is designed to compensate for the stochastic errors by estimating the azimuth error and the position error with two observations.

Several researchers attempt to use inertial navigation in construction, Joshua [31] applied accelerometers to classify workers' masonry activities in order to investigate workers' productivity. Taneja [32] investigated inertial measurement unit (IMU) sensors for location-tracking in a building site as compared to other sensors that were used to establish local area networks (WLAN) and radio frequency identification (RFID).

Although significant research attempts have been made in developing several indoor localization systems using various technologies, the performance of these systems is still expensive and not robust enough for usage in dense and noisy indoor environments such as construction jobsites. Further research work is needed to develop robust, cost-effective and accurate indoor localization solutions for supporting rugged construction applications, such as automated progress reporting and jobsite safety.

This paper presents a newly developed extension to the inertial navigation technique for indoor localization system using a microcontroller equipped with an inertial measurement unit (IMU). This extension is intended to reduce accumulated errors in measured acceleration and heading utilizing a jerk integration algorithm.

2. Developed method

The developed method encompassed hardware prototypes and software algorithms. The hardware development consists of a microcontroller equipped with an inertial measurement unit (IMU) and barometric pressure sensor as shown in Fig. 1.

The IMU incorporates three sensors—an ITG-3200 (MEMS triple-axis gyro), ADXL345 (triple-axis accelerometer), and HMC5883L (triple-axis magnetometer), which give 9 degrees of inertial measurement. The barometric pressure sensor provides the tenth degree of freedom for the system.

The outputs of all sensors are processed by an on-board ATmega328 processor and output over a serial interface. This hardware configuration provides 10 degrees of freedom to calculate the current position in three dimensional spaces as shown in Fig. 2.

The software development consists of three modules, namely: inertial measurement module, altitude measurement module and localization module as shown in Fig. 3. The inertial measurement module processes and fuses inertial sensors using a Direction Cosine Matrix (DCM) algorithm. This algorithm accounts for gyro drift correction using accelerometer (gravity) vector and the magnetometer (compass) vector, and compensates for tilt on X and Y magnetic components and provide correction for yaw angle magnetic heading. The altitude

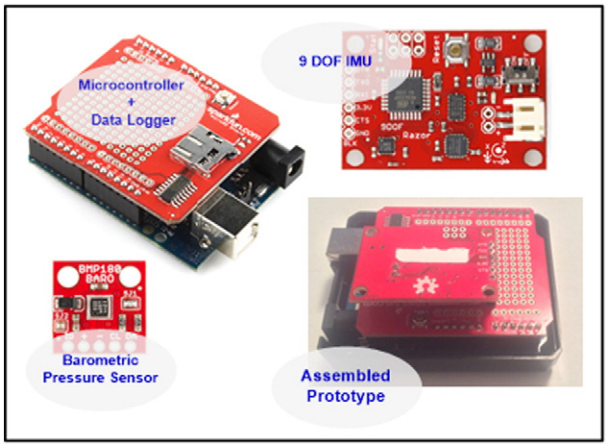

Fig. 1. Developed hardware prototype.

measurement module calculates the altitude based on the measured barometric pressure taking into account current weather condition (humidity, temperature, etc.).

The localization module calculates current position based on acceleration, heading and barometric pressure from the data acquisition module. The linear displacement is calculated using the displacement calculation algorithm by differentiation of the measured acceleration to calculate the jerk and then triple-integrates the jerk to calculate velocity and distance. The differentiation allows to correct DC margin errors in accelerometer readings and provides detection for detection of zero velocity intervals. The position estimation algorithm estimates current position based on calculated displacements, heading and altitude using extended Kalman filter. A detailed description of these algorithms is presented in the following sections with their mathematical background.

2.1. Displacement calculation algorithm.

Traditionally the displacement is calculated by double integration of acceleration, however the global displacement error will grow by time due to drift associated with DC bias in the acceleration signal. To minimize these errors, a triple integration approach is presented in this research, where the acceleration is first differentiated to calculate the rate of change of acceleration (jerk). The jerk also allows for removal of gravity acceleration components.

Jerk can be defined as the changing rate of acceleration with respect to time [33], and its international unit is m/s^3. According to Newton's second law of motion, jerk is viewed as the change of force magnitude for a unit mass in unit time. In recent years, jerk is applied in the tracking and positioning for Global Positioning System (GPS), the high-speed dynamic vehicle tracking, the automatic control of high-speed machines, and comfort evaluation for high speed trains and elevators [34–37]. It is obvious that the jerk and the integral of the displacement with respect to time also have determined an important significance.

The jerk value can be calculated by solving the time derivative of acceleration.

$$\text{Jerk} = \frac{d(\text{Acceleration})}{dt}. \tag{1}$$

Then the jerk is triple integrated using numerical integration method to obtain the acceleration, velocity, and displacement. Some traditional integration methods such as the Newmark method and Wilson-θ method are commonly used in earthquake engineering for jerk integration, however these methods assume that the acceleration is constant or linear variation during the interval of time [37,38], which will lead to the jerk in the interval, is assumed to be 0 or a

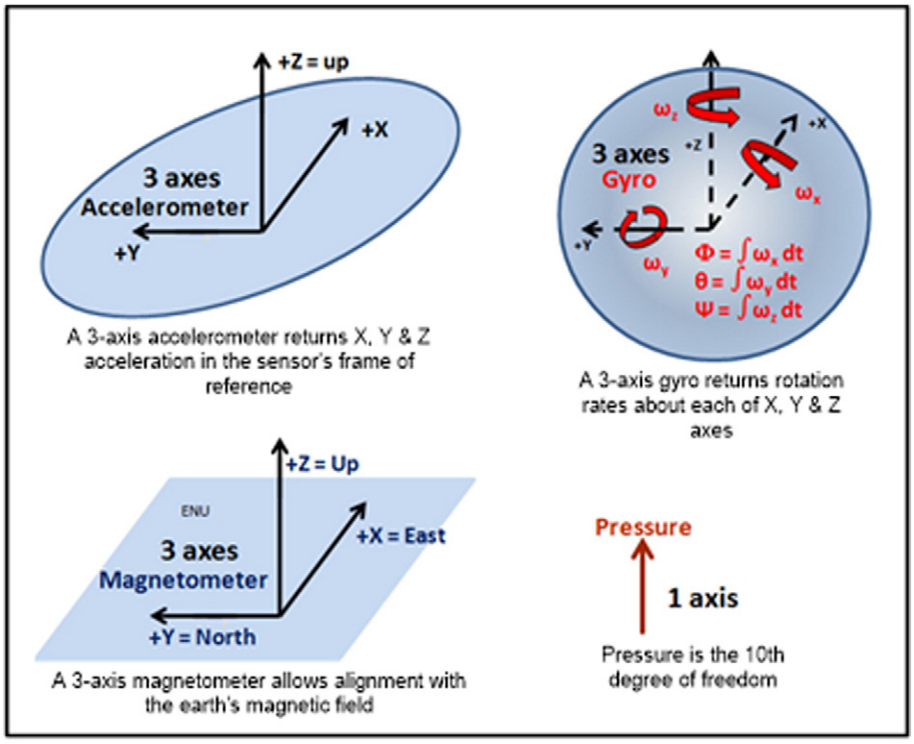

Fig. 2. 10 degrees of freedom measurement system.

constant, and this assumption is not in accordance with the real condition. In order to account for the variable acceleration and produce fewer errors than the normal integration, the trapeze integration method is used in this study.

$$\text{Acceleration}_t = \frac{(\text{Jerk}_{t-1} - \text{Jerk}_t)}{2} \times dt \tag{2}$$

2.2. Floor estimation

It is well known that atmospheric pressure decreases as altitude increases. Models for typical relationship between atmospheric pressure and altitude have been developed by many researchers. According to these models atmospheric pressure drops by about 0.11 hPa for every 1 m increase in height.

With the measured pressure P and the pressure at sea level P_0 e.g. 1013.25 hPa, the altitude in meters can be calculated with the international barometric formula:

$$\text{Altitude} = 44,330 \times \left(1 - \left(\frac{P}{P_0}\right)^{\frac{1}{5.255}}\right) \tag{3}$$

The reference sea level pressure is obtained for weather stations which report online their air pressure in real time with the height of the station.

While the process of estimating the altitude from the barometric pressure sensor seems straight forward, there are other issues that need to be taken into account. Barometric pressure sensors are normally calibrated for standard atmosphere conditions such as dry air with 15 °C

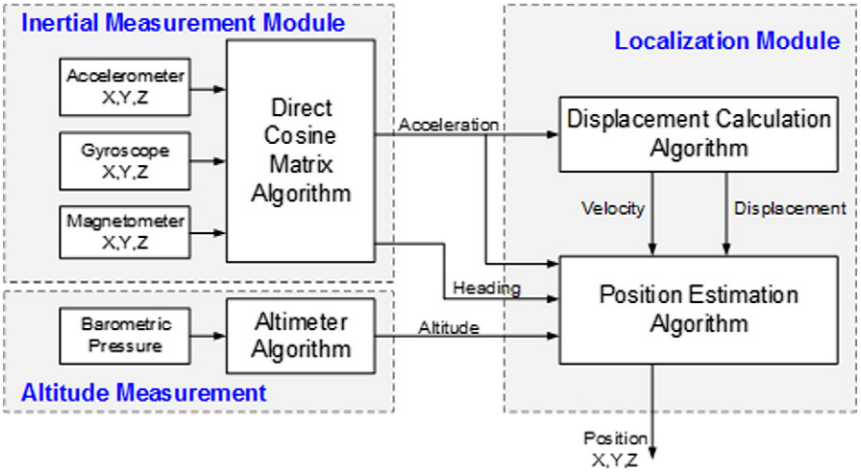

Fig. 3. Developed method.

temperature and 1013.2 hPa pressure. A correction factor must be considered for different weather conditions.

Also the latency of air pressure can cause a significant error in the sensor reading, however, in the case of indoor localization such factor can be neglected. Our testing indicated that there is about 0.42 hPa change in the air pressure due to a change of one floor, which is significantly larger than the sensor measurement noise (0.02 hPa for pressure sensor BMP180).

2.3. Position estimation algorithm.

The position estimation algorithm is based utilizes Kalman filter, which was first introduced in 1960 to present a solution for discrete data linear filtering problem [39]. Since then, extensive research and application had been proposed, particularly in the areas of robotics and navigation. The key advantage of the Kalman filter is its simple computational algorithm, and adaptive recursive nature [40]. Kalman filter estimation process is based on a feedback loop control system. Which first estimates the process's state at a point in time and then obtains feedback of measurements. This feedback measurement is used to adjust the model parameters for next estimate. The model assumes that the state of a system at a time t evolved from the prior state at time t-1 according to the equation

$$X_t = A_t X_{t-1} + B_t u_{t-1} + w_t \tag{4}$$

where X_t is the process state vector at time t, At is the state transition matrix which is applied to the previous state X_{t-1}, ut is the control input vector, B_t is the control–input model which is applied to the control vector u_t, and w_t is the process noise which is assumed to be drawn from a zero mean multivariate normal distribution with covariance Q_t.

At time t a measurement Z_t of the true state X_t is calculated according to

$$Z_t = H_t X_t + v_t \tag{5}$$

where H_t is the measurement model for mapping true state space into measurement space and v_t is the measurement noise which is assumed to be zero mean Gaussian white noise with covariance R_t.

The Kalman filter recursive estimator model as shown in Fig. 4 has two phases, the prediction phase, which estimates the priori process state at next observation time, and the correction phase, which incorporates a new measurement into the a priori estimate to obtain an improved a posterior estimate.

While the navigation problem at hand represents a non-linear system, the basic Kalman filter is limited to linear systems. Therefore the extended Kalman filter (EKF) is considered to address this problem. The EKF linearizes the non-linear system by using a first order Taylor expansion. The non-linear function f translates the state vector X at time step k − 1 to the next time step k, while the function h relates the current state to the measurement Z_k:

$$X_k = f(X_{k-1}, u_k) + W_k \tag{6}$$

$$Z_k = h(X_k) + V_k \tag{7}$$

The random variables W_k and V_k represent the noise of the state transition and the measurement. They are assumed to be white, mutually independent and normally distributed with covariance Q_k and R_k respectively.

The prediction stage equations are as follows:

- Predicted state estimate

$$\hat{X}_{k|k-1} = f\left(\hat{X}_{k-1|k-1}, u_k\right) \tag{8}$$

- Predicted covariance estimate

$$P_{k|k-1} = F_k P_{k-1|k-1} F_k^T + Q_k \tag{9}$$

The update stage equations are as follows:

- Innovation or measurement residual

$$\hat{Y}_k = Z_k - h\left(\hat{X}_{k|k-1}\right) \tag{10}$$

- Innovation (or residual) covariance

$$S_k = H_k P_{k|k-1} H_k^T + R_k \tag{11}$$

- Kalman gain

$$K_k = P_{k|k-1} H_k^T S_k^{-1} \tag{12}$$

- Updated state estimate

$$\hat{X}_{k|k} = \hat{X}_{k|k-1} + K_k \hat{Y}_k \tag{13}$$

- Updated covariance estimate

$$P_{k|k} = (I - K_k H_k) P_{k|k-1} \tag{14}$$

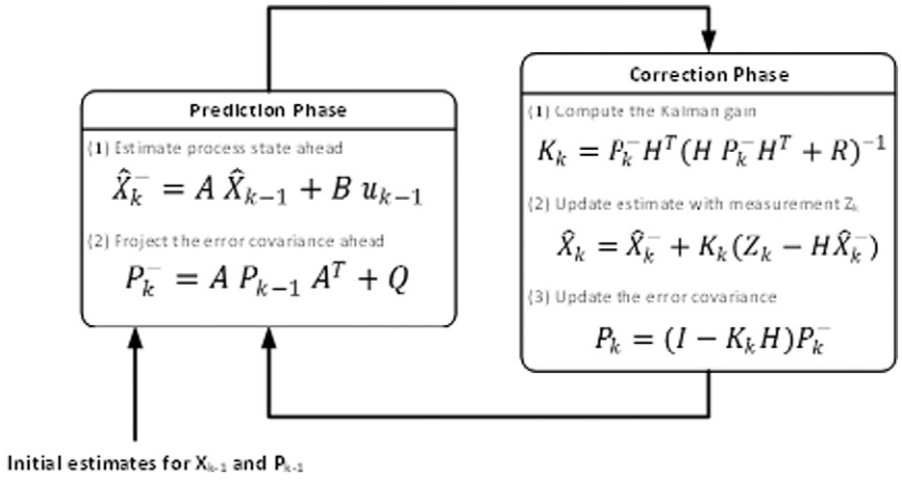

Fig. 4. Kalman filter recursive estimator model.

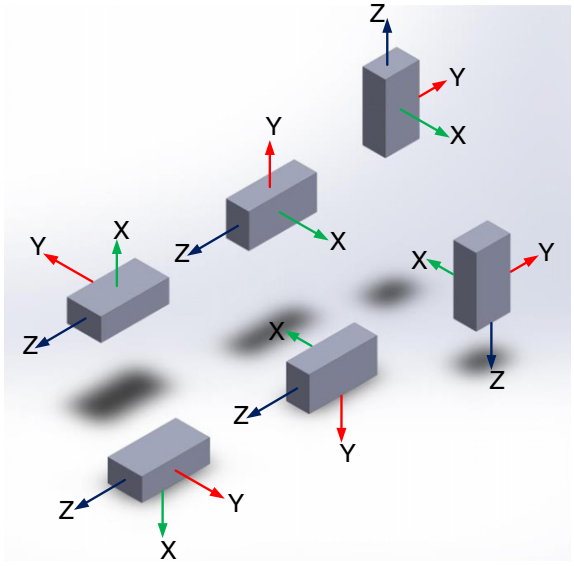

Fig. 5. Accelerometer calibration procedure.

where the state transition and observation matrices are defined to be the following Jacobians:

$$F_{k-1} = \left.\frac{\partial f}{\partial x}\right|_{\hat{X}_{k-1|k-1},u_k} \tag{15}$$

$$H_k = \left.\frac{\partial h}{\partial x}\right|_{\hat{X}_{k|k-1}} \tag{16}$$

In the context of the positioning algorithm described in this paper, the state vector x is a vector containing the position, velocity and acceleration data.

$$X = \left[x_k \;\; y_k \;\; z_k \;\; v_{xk} \;\; v_{yk} \;\; v_{zk} \;\; a_{xk} \;\; a_{yk} \;\; a_{zk}\right]^T \tag{17}$$

The process is started by making an appropriate, optimal estimate of the state vector at an initial epoch. The coordinates are set at the values of (0, 0, 0) while the velocities, accelerations and jerk are set at zero. Thereafter, at each epoch the following processes are repeated:

- Compute an estimate of the (predicted) state vector and its associated variance matrix from the optimal estimate of the state vector of the previous epoch.
- From the observation equations by combining the predicted state vector and the IMU measurements of the velocity and acceleration.

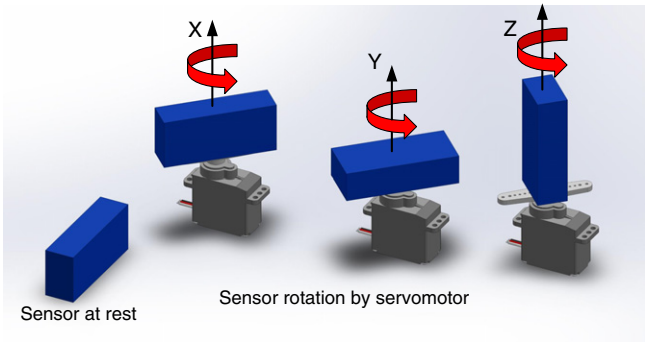

Fig. 6. Gyroscope calibration procedure.

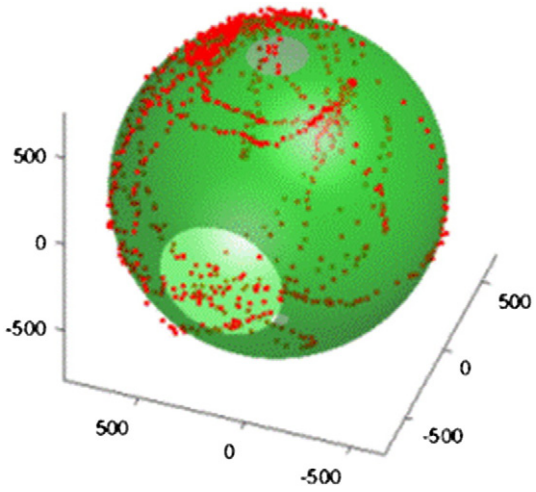

Fig. 7. Uncompensated magnetometer readings.

- Compute the estimate of the state vector and associated variance matrix.

3. IMU calibration

In order to improve the performance of the low cost IMU sensor, an effective method is implemented to calibrate the IMU. The method incorporates a multi-position scheme to calculate the scale factor matrix and the bias vector factors through Gauss–Newton nonlinear optimization. The factory calibration parameters are used as an initialization point for Newton's optimization, and after a few number of iterations, the algorithm converges to more accurate estimate of the sensor parameters. The mathematical model for the accelerometer output is described as:

$$A = S(V - O) \tag{18}$$

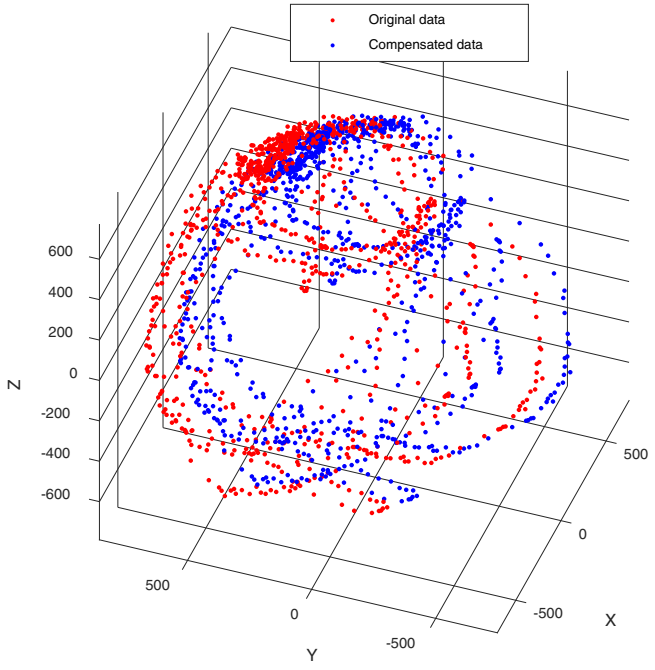

Fig. 8. Magnetometer readings before and after compensation.

Table 1
Experiments description.

Trial	Description	Duration	Distance
1	Slow straight line	7 s	5 m
2	Fast straight line	24 s	25 m
3	Running straight line	72 s	120 m
4	Campus walk	294 s	260 m
5	Outdoor campus walk	19 min	2610 m

where: A is the acceleration, V is the raw sensor measurement, S is the scale factor matrix and O is the bias vector.

The sensor's measurement limits are obtained by slowly moving it, in order to ensure that linear acceleration is not produced and all the measurement are from the earth gravity component. The sensor is placed in the six positions as shown in Fig. 5, and the readings of the minimum and maximum output values for the earth gravitation on each axis are recorded, in order to enable the initialization point for the optimization.

In static conditions, the modulus of the acceleration is equal to that of the gravity acceleration g. The sensor is placed in N different random static orientations and an error e_k is calculated:

$$e_k = a_x^2 + a_y^2 + a_z^2 - g^2 \tag{19}$$

The calibration parameters are calculated by minimizing the accumulated error for N readings an iterative optimization procedure that guarantees quadratic convergence.

For the gyroscope sensor, the calibration process is quite different, where the sensor will stay at rest to calculate the bias vector O. The scale factor matrix S is calculated using a servomotor with an optical encoder for precise rate control. In this approach, the gyroscope is rotated at preset angular rates while providing output measurements as shown in Fig. 6.

The magnetometer calibration compensates for hard and soft iron errors. Hard iron distortions are created by objects that produce a magnetic field. Soft iron distortions are considered deflections or alterations in the existing magnetic field. This type of distortion is commonly caused by metals such as nickel and iron. In most cases hard iron distortions will have a much larger contribution to the total uncorrected error than soft iron. Hard-iron effects are constant regardless of orientation or position of the sensor. These constant offsets can be calculated, stored and subtracted from the raw sensor data. Unlike hard-iron distortion, soft-iron distortion is the result of material that influences, or distorts, a magnetic field, but does not necessarily generate a magnetic field itself, and is therefore not additive.

A common way of visualizing and correcting hard and soft iron distortions is to plot the output of the magnetometer on a 3D graph. By rotating the sensor in a random way covering all the orientations, it produces a sphere of data points as shown in Fig. 7.

The magnetometer calibration procedure performs an ellipsoid fitting for the data and estimation of the compensation factors, where the output of the magnetometer is shown in Fig. 8. It is clear that the calibration process removed the offset in the magnetometer measurements.

4. Experiments and results

To examine the effectiveness of the developed method, several experiments have been performed for different localization scenarios. The developed prototype was mounted on using a belt clip on a human volunteer. The prototype processed the data and sent the personnel position wirelessly to a database application, which in turn stored the data with timestamps.

Experiments were performed in indoor laboratory environment at Concordia University, Construction Management Lab. Another set of experiments was performed in the corridors of Concordia University at Sir George Williams Campus. The experiment settings are summarized in Table 1. In these experiments, different paths were used for distance ranges from 5 m to 260 m. Different walking patterns were performed ranging from slow, fast to running, in order to check the consistency of the developed method.

In the campus walk experiment the path starts and ends at the same position. The path includes straight line walking and had several left and right turns. Also the path included climbing up and down several flights of stairs to check the accuracy of altitude measurement using the barometric pressure sensor signal as shown in Fig. 9. Experiments (1–4) were repeated thirty times to appropriately assess the results, with a total of 120 data sets collected, and a total experimentation duration of 396 min. Experiment no. 5 was repeated 4 times.

The effect of the jerk integration on the removal of the velocity bias is shown in Fig. 10, where the velocity in the x-axis before the jerk integration shows a drift in the calculated velocity, and such drift is one of the reasons for the accumulated errors in the calculated position. The jerk integrator removed the constant bias in the velocity, and hence reduced the errors in position estimation.

Reducing errors in acceleration calculation through integration of the jerk, provides an effective way to remove gravity component in the measured acceleration and orientation errors, which cause huge drift error on long runs. An error in IMU orientation also could cause an incorrect projection of the acceleration signals onto global axes, which in turn causes wrong integration direction of the acceleration.

Fig. 9. Campus walk path.

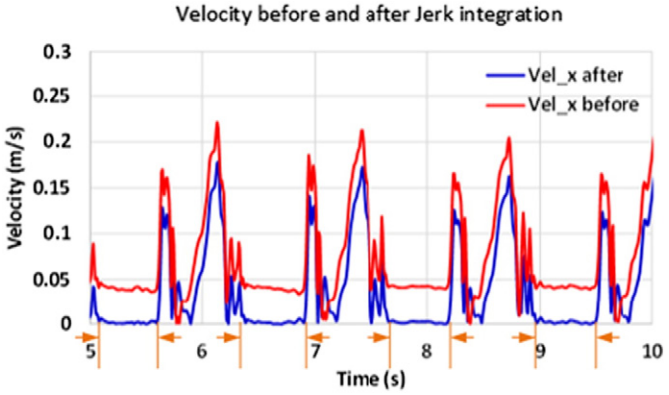

Fig. 10. Velocity before and after jerk integration.

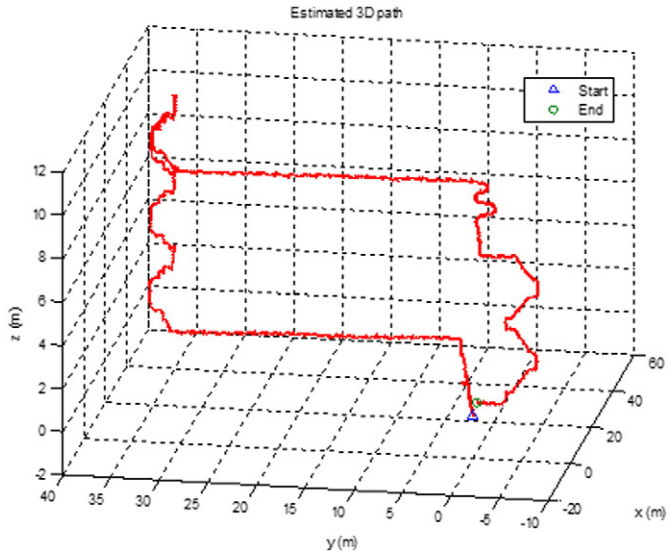

Fig. 11. Estimated 3D travel path.

The 3D plot of the estimated walking path of experiment no. 4 is shown in Fig. 11, where the 2D distance error between the start and the end was 2.98 m over the 260.79 m total path length. Hence the distance estimation error is about 1.14% of the total traveled distance.

The average drift error (as a percentage of the total traveled path length) for all experiments ranged from 0.28% for experiment trial 1 to 1.14% for experiment trial 4 (an average of 30 runs). These errors are compared with Taneja [32], where an off the shelf IMU localization system was utilized. Their experimental results showed a range of drift error from 1.92% to 6.2% for travel paths with length up to 250 m. It is clear that our developed method is able to estimate indoor position with higher accuracy.

In order to evaluate the developed method in longer duration and distance experiments, a 2.6 km walk experiment was conducted on the campus of the University of Waterloo. The ground truth measurements were collected using GPS and compared to the results of the developed method as shown in Fig. 12. In this experiment the two Kalman filters were utilized to compare the results. The linear Kalman filter (LKF) estimated the distance with an accumulated error of 11.19%, while the extended Kalman filter (EKF) estimated the distance with a total accumulated error of 4.67% of the total traveled distance.

5. Conclusions

A method for indoor localization was presented in this paper, which made use of a microcontroller equipped with IMU and a barometric pressure sensor for 10 degrees of freedom position estimation in three dimensional spaces. This method employs jerk integration algorithm for high accuracy displacement calculation, and reduction of accumulated drift errors in the measured acceleration and heading signals. The IMU contains a cluster of three sensors: 3 axis accelerometer, gyroscope, and magnetometer. A direct cosine matrix algorithm was utilized to fuse the data of the sensors' cluster and provide reliable estimates of non-gravitational acceleration, altitude and heading. The 3D location was estimated using extended Kalman filter algorithm, to linearize the non-linear system using a first order Taylor expansion. The developed method was tested on several indoor and outdoor experiments, where the results showed an average drift error ranging from 0.28% to 4.67% of the total traveled distances.

The results presented in this study demonstrate the potential of utilizing IMUs in location estimation and tracking on indoor construction jobsites. The developed method can be used to obtain location information with respect to construction resources (labor, materials, and equipment), which is essential for scalable near-real-time decision-making, timely tracking of project's status and proactive safety monitoring on construction projects. The developed method could be used on a wide range of construction projects ranging from buildings, tunnels, to other GPS denied areas of all sizes and locations. The developed method can be expanded to encompass radio frequency modules to account for Received Signal Strength (RSS), which can add more accuracy to the location estimation in indoor construction job sites, and in a cost-effective manner.

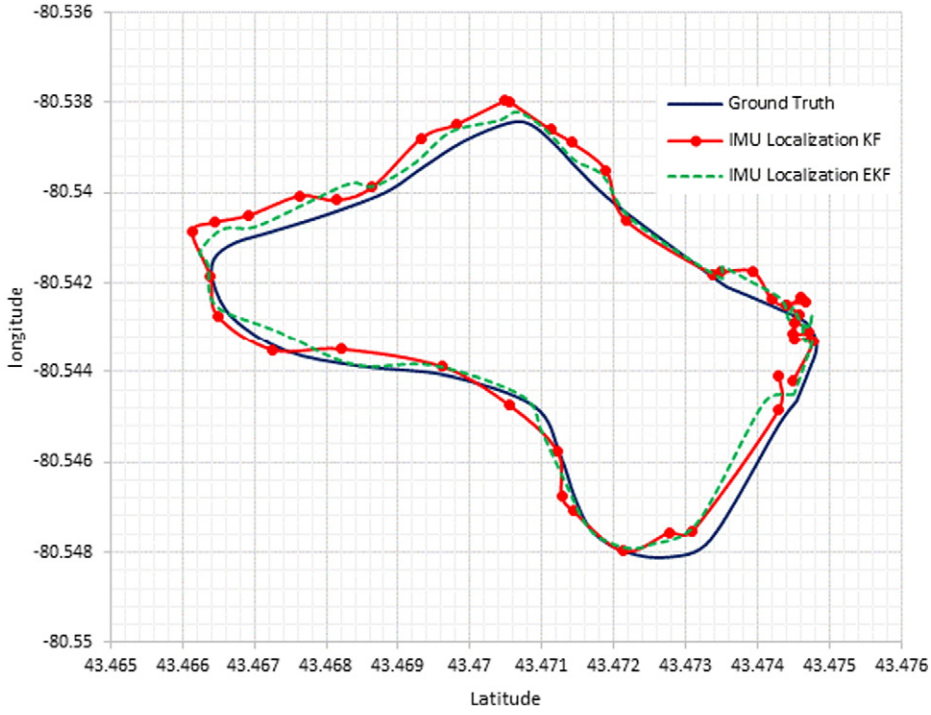

Fig. 12. Experiment no. 5 (outdoor campus walk).

References

[1] C.H. Caldas, D.G. Torrent, C.T. Haas, Using global positioning system to improve materials-locating processes on industrial projects, J. Constr. Eng. Manag. 132 (7) (2006) 741–749, http://dx.doi.org/10.1061/(ASCE)0733-9364(2006)132:7(741).

[2] E. Ergen, B. Akinci, R. Sacks, Tracking and locating components in a precast storage yard utilizing radio frequency identification technology and GPS, Autom. Constr. 16 (3) (2007) 354–367, http://dx.doi.org/10.1016/j.autcon.2006.07.004.

[3] P.M. Goodrum, M.A. McLaren, A. Durfee, The application of active radio frequency identification technology for tool tracking on construction job sites, Autom. Constr. 15 (3) (2006) 292–302, http://dx.doi.org/10.1016/j.autcon.2005.06.004.

[4] D.G. Torrent, C.H. Caldas, Methodology for automating the identification and localization of construction components on industrial projects, J. Comput. Civ. Eng. 23 (1) (2009) 3–13, http://dx.doi.org/10.1061/(ASCE)0887-3801(2009)23:1(3).

[5] W. Jang, M.J. Skibniewski, A wireless network system for automated tracking of construction materials on project sites, J. Civ. Eng. Manag. 14 (1) (2008) 11–19, http://dx.doi.org/10.3846/1392-3730.2008.14.11-19.

[6] H.M. Khoury, V.R. Kamat, High-precision identification of contextual information in location-aware engineering applications, Adv. Eng. Inform. 23 (4) (2009) 483–496, http://dx.doi.org/10.1016/j.aei.2009.04.002.

[7] S.N. Razavi, C.T. Haas, Multisensor data fusion for on-site materials tracking in construction, Autom. Constr. 19 (8) (2010) 1037–1046, http://dx.doi.org/10.1016/j.autcon.2010.07.017.

[8] S.N. Razavi, D.A. Young, H. Nasir, C. Haas, C. Caldas, P. Goodrum, P. Murray, Field trial of automated material tracking in construction, Annual Conference of the Canadian Society for Civil Engineering 2008—"Partnership for Innovation", June 10, 2008–June 13, 3 2008, pp. 1503–1511.

[9] J. Song, C.T. Haas, C. Caldas, E. Ergen, B. Akinci, Automating the task of tracking the delivery and receipt of fabricated pipe spools in industrial projects, Autom. Constr. 15 (2) (2006) 166–177, http://dx.doi.org/10.1016/j.autcon.2005.03.001.

[10] J. Teizer, M. Venugopal, A. Walia, Ultra wideband for automated real-time three-dimensional location sensing for workforce, equipment, and material positioning and tracking, Transp. Res. Rec. 2081 (2008) 56–64, http://dx.doi.org/10.3141/2081-06.

[11] K. Finkenzeller, RFID Handbook: Fundamentals and Applications in Contactless Smart Cards and Identification, Wiley, West Sussex, UK, 2003.

[12] J.R. Guerrieri, M.H. Francis, P.F. Wilson, T. Kos, L.E. Miller, N.P. Bryner, L. Klein-Berndt, RFID-assisted indoor localization and communication for first responders, European Conference on Antennas and Propagation: EuCAP 2006, November 6, 2006–November 10 2006, p. 626 SP.

[13] R. Want, A. Hopper, V. Falcao, J. Gibbons, Active badge location system, ACM Trans. Inf. Syst. 10 (1) (1992) 91–102, http://dx.doi.org/10.1145/128756.128759.

[14] M.J. Skibniewski, W. Jang, Localization technique for automated tracking of construction materials utilizing combined RF and ultrasound sensor interfaces, 2007 ASCE International Workshop on Computing in Civil Engineering, July 24, 2007–July 27 2007, pp. 657–664, http://dx.doi.org/10.1061/40937(261)78.

[15] B. Kim, J. Choi, Active beacon system with the fast processing architecture for indoor localization, 12th IEEE International Conference on Emerging Technologies and Factory Automation, ETFA 2007, September 25, 2007–September 28 2007, pp. 892–895, http://dx.doi.org/10.1109/EFTA.2007.4416875.

[16] J. Hightower, G. Borriello, Location systems for ubiquitous computing, Computer 34 (8) (2001) 57–66, http://dx.doi.org/10.1109/2.940014.

[17] P. Bahl, V.N. Padmanabhan, RADAR: an in-building RF-based user location and tracking system, 19th Annual Joint Conference of the IEEE Computer and Communications Societies—IEEE INFOCOM2000: 'Reaching the Promised Land of Communications', March 26, 2000–March 30, 2 2000, pp. 775–784.

[18] E. Elnahrawy, X. Li, R.P. Martin, The limits of localization using signal strength: a comparative study, 2004 First Annual IEEE Communications Society Conference on Sensor and Ad Hoc Communications and Networks 2004, pp. 406–414.

[19] T.P. Deasy, W.G. Scanlon, Stepwise algorithms for improving the accuracy of both deterministic and probabilistic methods in WLAN-based indoor user localisation, Int. J. Wireless Inf. Networks 11 (4) (2004) 207–216, http://dx.doi.org/10.1007/s10776-004-1234-1.

[20] J. Hightower, R. Want, G. Borriello, SpotON: An indoor 3D location sensing technology based on RF signal strength, UW CSE 00-02-02, University of Washington, Department of Computer Science and Engineering, Seattle, WA, 2000.

[21] L.M. Ni, Y. Liu, C.L. Yiu, A.P. Patil, LANDMARC: indoor location sensing using active RFID, Proceedings of the First IEEE International Conference on Pervasive Computing and Communications (PerCom 2003) 2003, pp. 407–415.

[22] A. Pradhan, E. Ergen, B. Akinci, Technological assessment of radio frequency identification technology for indoor localization, J. Comput. Civ. Eng. 23 (4) (2009) 230–238, http://dx.doi.org/10.1061/(ASCE)0887-3801(2009)23:4(230).

[23] H. Liu, H. Darabi, P. Banerjee, J. Liu, Survey of wireless indoor positioning techniques and systems, IEEE Trans. Syst. Man Cybern. Part C Appl. Rev. 37 (6) (2007) 1067–1080, http://dx.doi.org/10.1109/TSMCC.2007.905750.

[24] R. Reimann, A. Bestmann, M. Ernst, Locating technology for AAL applications with direction finding and distance measurement by Narrow Bandwidth Phase Analysis, Evaluating AAL Systems Through Competitive Benchmarking: International Competitions and Final Workshop, EvAAL 2012, July and September 2012. Revised Selected Papers (vol. 362, p. 52), Springer, 2013.

[25] R. Sim, G. Dudek, Comparing image-based localization methods, 18th International Joint Conference on Artificial Intelligence, IJCAI 2003, August 9, 2003–August 15 2003, pp. 1560–1562.

[26] C. Randell, C. Djiallis, H. Muller, Personal position measurement using dead reckoning, 7th IEEE International Symposium on Wearable Computers, ISWC 2003, October 21, 2003–October 23 2003, pp. 166–175.

[27] Arthur Gelb, Applied Optimal Estimation, MIT press, 1974.

[28] G. Glanzer, T. Bernoulli, T. Wiessflecker, U. Walder, Semi-autonomous indoor positioning using MEMS-based inertial measurement units and building information, 2009 6th Workshop on Positioning, Navigation and Communication (WPNC'09) 2009, pp. 135–139, http://dx.doi.org/10.1109/WPNC.2009.4907816.

[29] W.N. Chai, C. Chen, E. Edwan, Enhanced indoor navigation using fusion of IMU and RGB-D camera, International Conference on Computer Information Systems and Industrial Applications, Atlantis Press, 2015.

[30] Z. Zheng, S. Han, J. Yue, L. Yuan, Compensation for stochastic error of gyros in a dual-axis rotational inertial navigation system, J. Navig. 69 (01) (2016) 169–182.

[31] L. Joshua, K. Varghese, Accelerometer-based activity recognition in construction, J. Comput. Civ. Eng. 25 (5) (2011) 370–379, http://dx.doi.org/10.1061/(ASCE)CP.1943-5487.0000097.

[32] S. Taneja, A. Akcamete, B. Akinci, J.H.J. Garrett, L. Soibelman, E.W. East, Analysis of three indoor localization technologies for supporting operations and maintenance field tasks, J. Comput. Civ. Eng. 26 (6) (2012) 708–719, http://dx.doi.org/10.1061/(ASCE)CP.1943-5487.0000177.

[33] S.H. Schot, Jerk: the time rate of change of acceleration, Am. J. Phys. 46 (11) (1978) 1090–1094, http://dx.doi.org/10.1119/1.11504.

[34] T. Aoki, Y. Shimogaki, T. Ikki, M. Tanikawara, S. Sugimoto, Y. Kubo, K. Fujimoto, Cycle slip detection in kinematic GPS with a jerk model for land vehicles, Int. J. Innov. Comput. Inf. Control. 5 (1) (2009) 153–166.

[35] C. Liu, D.C. Gazis, T.W. Kennedy, Human judgment and analytical derivation of ride quality, Transp. Sci. 33 (3) (1999) 290–297, http://dx.doi.org/10.1287/trsc.33.3.290.

[36] D. Hrovat, M. Hubbard, A comparison between jerk optimal and acceleration optimal vibration isolation, J. Sound Vib. 112 (2) (1987) 201–210, http://dx.doi.org/10.1016/S0022-460X(87)80189-X.

[37] R.W. Clough, J. Penzien, Dynamics of Structures, McGraw- Hill, New York, NY, USA, 1993.

[38] A.K. Chopra, Dynamics of Structures: Theory and Applications to Earthquake Engineering, Prentice-Hall, New Delhi, India, 2007.

[39] R.E. Kalman, A new approach to linear filtering and prediction problems, J. Basic Eng. 82 (1) (1960) 35–45.

[40] B.D.O. Anderson, J.B. Moore, Optimal Filtering, Courier Corporation, 2012.